Quantum Hall solitons with intertwined spin and pseudospin at $\nu=1$

Sankalpa Ghosh* and R. Rajaraman[†]

School of Physical Sciences, Jawaharlal Nehru University, New Delhi 110067, India

(Received 13 January 2000; revised manuscript received 1 August 2000; published 22 December 2000)

In this paper we study in detail different types of topological solitons that are possible in bilayer quantum Hall systems at filling fraction $\nu=1$ when spin degrees of freedom are included. Starting from a microscopic Hamiltonian we derive an effective energy functional for studying such excitations. The gauge invariance and CP^3 character of this energy fuctional and their consequences are examined. Then we identify permissible classes of finite energy solutions that are topologically nontrivial. We also numerically evavluate a representative solution in which a pseudospin (layer degrees of freedom) bimeron in a given spin component is intertwined with spin skyrmions in each layer and discuss whether it is energetically favored as the lowest-lying excitation in such system with some numerical results.

I. INTRODUCTION

Systems that permit topological excitations, i.e., where field configurations can be classifield by homotopy sectors characterized typically by some winding number, have been studied in a general sense in mathematical physics for a long time. That such interesting possibilities can actually arise and play a significant role in the quantum Hall physics was demonstrated in the work of of Sondhi *et al.*[1] They showed that, for example, in a single-layer Hall liquid at filling factor $\nu=1$, the lowest energy excitations in spin for low Zeeman coupling are the so-called skyrmions and not single spin flips. These skyrmions are topological excitations in the spin texture, in which the spin starts being, say, ''up'' at the origin and as you go outwards, starts tilting down in a flared manner to become asymptotically ''down'' spin at large distances. Subsequently experimental support for the existence of such excitations was also discovered in NMR measurements.[2]

Meanwhile quantum Hall phenomena have also been studied in double-layer systems.[3,4] The double-well Hall plateaus at unit filling can be understood by associating with each electron a ''pseudospin'' in addition to its lowest Landau level (LLL) orbital wave function.[5,6] The up and down components of this pseudospinor give the probability amplitudes for the electron being in the upper and lower layer, respectively. The ground state of the $\nu=1$ double-layer system, known to be a quantum Hall state with a Hall conductivity plateau, is a pseudospin ferromagnet with the pseudospin aligned in the x direction. This is a very remarkable phenomenon in that it amounts to interlayer coherence between the electrons in the two layers. This pseudospin degree of freedom is in addition to physical spin. To start with, in analyzing double-layer phenomena, the spin degrees of freedom are suppresed for simplicity. Even then one can still consider excitations in the pseudospin. Inspired by the presence of skyrmions in spin, people have also considered the possibility of topological excitations in pseudospin. Such pseudospin textures called ''merons'' and ''bimerons'' have been suggested as possible low-lying excitations of double-layer systems.[5] The homotopy group $\pi_2[S_2]$ and its winding number are identical for spin and pseudospin since mathematically pseudospin is identical to spin, both being SU(2)

spinor fields on a plane. The change in terminology from skyrmions to bimerons does not indicate any topological difference between the two in going from spin to pseudospin excitations but only differences in their detailed profiles. This difference in turn happens because of the difference in the energetics of spin and pseudospin and correspondingly, their asymptotic direction. Meron excitations, if present in double layers, can give rise to a Kosterlitz-Thouless[7] (KT) transition, which may enable them also to be experimentally observable.

Clearly there are prospects of even more esoteric excitations when both spin and pseudospin degrees of freedom are considered simultaneously. That is the theme of this present work. We will continue to study the unit filling factor ($\nu=1$) case. There has already been some discussion of the combined spin-pseudospin $\nu=1$ double-layer system.[8,9] Our work discusses different aspects of the problem than these studies. We analyze in substantive detail intertwined spin-pseudospin topological excitations of this system. When both spin and pseudospin are active degrees of freedom, these are together described by a four-component object. This four-component object has been referred to as a CP^3 spinor in the literature.[9] That is correct, but needs to be justified. A theory does not become a CP^3 theory just because its field is a normalized four-component object. The system must obey a U(1) gauge invariance, which is what makes the spinors span a projective space, implied in the acronym CP. Without that gauge invariance the results on CP^N in the literature[10,11] cannot be borrowed and applied.

So we begin in Sec. II by showing, starting from the basic microscopic theory of the $\nu=1$ system that in the effective LLL theory for the spin-pseudospin texture such gauge invariance *is* there. This is a straightforward derivation following the procedure developed by Moon *et al.*[6] In fact we find that in the limit where the layer separation d vanishes, the Coulomb interaction energy is precisely the prototype CP^3 Euclidean action used in the pioneering papers on that topic,[10] for which exact topological solutions are known in terms of analytic functions. Of course, when $d\neq0$, the energy functional is more complicated and these analytical solutions do not hold. But the theory is still a CP^3 theory, and the homotopy classification of the solutions still hold. Only the solutions themselves have to be calculated numerically.

A topologically nontrivial CP^3 solution will generally involve an intertwined texture in the physical spin in each layer as well as in the pseudospin of each physical spin projection. One can ask whether such solutions can be legitimately interpreted as containing, as subsystems, spin skyrmions in either or both of the layers, possibly intertwined with a pseudospin meron or bimeron. If so, then such possibilities of containing several topological entities as subsystems has to be made compatible with the fact that any finite energy CP^3 texture carries altogether *only one* topological winding number. We study all these questions in Sec. III and find that there are certain restrictions on the types of solutions permitted. We show that the individual layers of a double-layer system cannot accomodate all possible spin structures one may find in a pair of unrelated single layers. The spin-winding numbers in the two layers are related to one another and to the pseudospin winding number.

Consistent with these restrictions, we then pick in Sec. IV a representative ansatz that can be viewed as a spin skyrmion intertwined with a pseudospin bimeron. We then numerically evaluate such a solution by solving the coupled nonlinear partial differential equations that arise from extremizing the texture energy functional. In earlier work[12,13] we had studied in some detail both meron and bimeron excitations in pseudospin for double layer systems, with the spin degree of freedom suppressed. The present calculation is a more complicated version with CP^3 spinors, but is done by similar numerical techniques. We present the spin and pseudospin profiles of our intertwined solutions for different values of interlayer separation.

We also estimate the interaction energy of these solutions for some typical sets of values of system parameters. We discuss the dependence of this energy on the separation between the two meron centers. We find, as expected, that if only the gradient and capacitance energies are considered, their minimization will drive the textures towards zero size. Therefore we also calculate the topological charge-dependent Coulomb energy of our solutions which, being repulsive, should drive the merons farther apart, offsetting the above-noted tendency towards zero size. Then we extremize the total energy so obtained and find that it does show a minimum at some optimal meron separation, for each value of layer separation.

We also find that these energies are approximately of the same order as those of purely spin skyrmions of the single-layer system. We make qualitative speculations on whether or not our spin-pseudospin intertwined solitons can be energetically favored over solitons purely in spin or pseudospin, or over simple spin flips.

II. TEXTURE ENERGY AND ITS GAUGE INVARIANCE

In a double-layer quantum Hall system with both spin and pseudospin degrees of freedom present, an electron will carry, apart from its coordinate wave function $\phi_X(\vec{r})$, a four-component normalized spinor whose components in general may vary with the orbital quantum number X. For any given X, this spinor can be denoted by

$$a_\sigma(X) = \begin{pmatrix} a_1(X) \\ a_2(X) \\ a_3(X) \\ a_4(X) \end{pmatrix}, \tag{2.1}$$

where the spin-pseudospin index $\sigma = 1,2,3,4$ corresponds to amplitudes that the electron is in the upper-layer up-spin, upper-layer down-spin, lower-layer up-spin, and lower-layer down-spin states, respectively. It will henceforth be understood that the spinor is normalized, i.e., $\Sigma_\sigma |a_\sigma(X)|^2 = 1$ for each X. In the literature, this a_σ has sometimes been referred to as a CP^3 spinor (see, for instance, Ezawa[9]). That is correct, but requires a little justification. In a CP^3 theory, the spinor must not only be a normalized four-component object, but be defined only modulo a local gauge transformation common to all four components. This in turn requires that the Euclidean action or static energy functional of the spinor field enjoys a corresponding gauge invariance. In this section we will verify all this. We will also see that the nature of the gauge symmetry is different for a double-layer system than for a pair of isolated single layers. This, as we shall see, has the important consequence of prohibiting certain topological spin excitations in the double-layer system that would have been present in the individual layers had they been far apart. In this way, along with establishing the CP^3 nature of the system, we will also identify permissible types of excitations where the spin and pseudospin are nontrivially intertwined, some of which we numerically evaluate in later sections.

Let us start by deriving the energy functional of any spin-pseudospin texture from the microscopic Hamiltonian. This is just a straightforward generalization of the procedure already in the literature for the simpler case of a spinless bilayer problem.[6] Therefore we need to present only the essential equations needed for completeness and understandability. We take the microscopic Hamiltonian to be

$$H = H_K + H_1 + H_C. \tag{2.2}$$

Here

$$H_K = \frac{1}{2m} \sum_{\sigma=1}^{4} \int d\vec{r} \, \psi_\sigma^\dagger D^2 \psi_\sigma \tag{2.3}$$

is the kinetic energy in the presence of the magnetic field. We will be working at $\nu = 1$ in the lowest Landau level (LLL) approximation. Corespondingly, the operator $\psi_\sigma(\vec{r})$ is the LLL-projected electron field operator expanded in terms of lowest Landau level orbitals as

$$\psi_\sigma(\vec{r}) = \sum_{X=1}^{N} \phi_X(\vec{r}) C_{\sigma X}, \tag{2.4}$$

with $\phi_X(\vec{r})$ being a LLL orbital, say, in the Landau gauge with X as its guiding center.

The second term in the Hamiltonian is the one-body term representing the Zeeman and interlayer tunneling energies.

$$H_1 = \sum_{\sigma,\delta} \int d\vec{r}\, \psi_\sigma^\dagger(\vec{r})(\tilde{g}\hat{\sigma}_z - t\hat{\tau}_x)_{\sigma\delta}\psi_\delta(\vec{r}), \quad (2.5)$$

where $\hat{\sigma}_z$ and $\hat{\tau}_x$ are spin and pseudospin matrices suitably generalized as 4×4 matrices on the outer product space of spin and pseudospin.

The third term in the Hamiltonian is the Coulomb term:

$$H_C = \frac{1}{2} \sum_{\sigma_1,\sigma_2=1}^{4} \int d\vec{r}_1\, d\vec{r}_2\, \psi_{\sigma_1}^\dagger(\vec{r}_1)\psi_{\sigma_2}^\dagger(\vec{r}_2)V^{\sigma_1\sigma_2}$$

$$\times (\vec{r}_1 - \vec{r}_2)\psi_{\sigma_2}(\vec{r}_2)\psi_{\sigma_1}(\vec{r}_1). \quad (2.6)$$

In the above, the Coulomb potential $V^{\sigma_1\sigma_2}$ depends on whether the particles are in the same layer or different layers,

$$V^{\sigma_1\sigma_2} = v^s \equiv \frac{e^2}{\epsilon r_{12}}, \quad \sigma_1,\sigma_2 \text{ in the same layer,}$$

$$V^{\sigma_1\sigma_2} = v^d \equiv \frac{e^2}{\epsilon\sqrt{r_{12}^2 + d^2}}, \quad \sigma_1,\sigma_2 \text{ in different layers}$$

$$(2.7)$$

where d is the interlayer distance. To obtain the energy of an arbitrary spin-pseudospin texture, we adopt the strategy followed in the work of Moon *et al.*[6] We first consider the ansatz state

$$|\Psi\rangle = \prod_X \left[\sum_\sigma C_{\sigma X}^\dagger a_\sigma(X) \right] |0\rangle, \quad (2.8)$$

where $|0\rangle$ is the vacuum (no electron) state, X stands for Landau gauge orbitals, and $a_\sigma(X)$ is an orbital-dependent four-spinor as in Eq. (2.1). In the high-B limit each Landau gauge orbital density is uniform along the y axis with support on a thin line localized around some value of x. Further these states are closely spaced along the x direction. Using this feature, we will later on replace the orbital label X by the x coordinate itself. In that case the above texture $a_\sigma(X)$ depends only on the x coordinate and not on y, and therefore carries zero topological number density [see Eq. (3.14) below]. Nevertheless we will use this ansatz to calculate its energy functional, and then later that energy functional to the more general and topologically nontrivial textures by invoking isotropy of the system in the x-y plane. This was exactly the strategy used in Ref. 6. We will calculate the energy functional of the spin-pseudospin texture (2.8) by taking the mean value of the second quantized Hamiltonian in that state.

At unit filling $\nu = 1$, and in the space of LLL orbitals, the kinetic term H_K is just a constant equal to $(N/2)\hbar\omega$, the energy of the filled LLL band. This constant will henceforth be neglected.

The Zeeman and tunneling one-body energies yield

$$E_1[a_\sigma(X)] = \sum_X \{\tilde{g}[|a_1(X)|^2 - |a_2(X)|^2$$

$$+ |a_3(X)|^2 - |a_4(X)|^2]$$

$$- t[a_1(X)a_3^*(X) + a_2(X)a_4^*(X) + \text{c.c.}]\}. \quad (2.9)$$

The expectation value of the Coulomb interaction Hamiltonian can be conveniently written in terms of the following spinorial bilinears for the upper (u) and lower (l) layers:

$$F_u(X) = |a_1(X)|^2 + |a_2(X)|^2, \quad (2.10)$$

$$F_l(X) = |a_3(X)|^2 + |a_4(X)|^2, \quad (2.11)$$

$$G_u(X_1,X_2) = \sum_{i=1,2} a^i(X_1)a^{i*}(X_2), \quad (2.12)$$

$$G_l(X_1,X_2) = \sum_{i=3,4} a^i(X_1)a^{i*}(X_2). \quad (2.13)$$

On inserting H_C from Eq. (2.6) and the state Ψ from Eq. (2.8) straightforward algebra then gives us the Coulomb energy in terms of the spinors a_σ:

$$E_C[a_\sigma(X)] \equiv \langle\Psi|H_C|\Psi\rangle = \langle H_C\rangle_{direct} - \langle H_C\rangle_{exchange}, \quad (2.14)$$

with

$$\langle H_C\rangle_{direct} = \frac{1}{2} \sum_{X_1,X_2} \{D^s + (D^d - D^s)[F_u(X_1)F_l(X_2)$$

$$+ F_l(X_1)F_u(X_2)]\} \quad (2.15)$$

and

$$\langle H_C\rangle_{exchange} = \frac{1}{2} \sum_{X_1,X_2} [E^s(|G_u|^2 + |G_l|^2)$$

$$+ E^d(G_u^*G_l + G_uG_l^*)]. \quad (2.16)$$

Here

$$D^{s,d}(X_2 - X_1) = V_{X_1,X_2,X_1,X_2}^{s,d},$$

$$E^{s,d}(X_2 - X_1) = V_{X_2,X_1,X_1,X_2}^{s,d}, \quad (2.17)$$

with

$$V_{X_1,X_2,X_3,X_4}^{sd} = \int d\vec{r}_1\, d\vec{r}_2\, V^{s,d}(\vec{r}_1 - \vec{r}_2)$$

$$\times \phi_{X_1}^*(\vec{r}_1)\phi_{X_2}^*(\vec{r}_2)\phi_{X_3}(\vec{r}_1)\phi_{X_4}(\vec{r}_2). \quad (2.18)$$

These direct and exchange Coulomb interaction matrix elements $D^{s,d}$ and $E^{s,d}$ between two electrons in LLL orbitals X_1 and X_2, in the same (s) or different (d) layers, are exactly the same as were used in the spinless double-layer problem by Moon *et al.*[6] However, the inclusion of the physical spin

degrees of freedom is reflected in the energy expressions in Eqs. (2.15) and (2.16), which involve all four components of the spin-pseudospin multiplet a_σ.

Adding the contributions in Eq. (2.14) and Eq. (2.9) we get the total energy expectation value

$$E[a_\sigma(X)] = E_1[a_\sigma(X)] + E_C[a_\sigma(X)]. \qquad (2.19)$$

In the Hartree-Fock approximation, this energy expectation value $E[a_\sigma(X)]$ in Eq. (2.14) will be minimized to get the ground-state and excited-state spin-pseudospin textures.

But, let us first examine the gauge invariance of the energy functional $E[a_\sigma(X)]$. Consider the transformation

$$a_\sigma(X) \to e^{i\Lambda_u(X)} a_\sigma(X) \quad \text{for} \quad \sigma = 1,2$$

$$a_\sigma(X) \to e^{i\Lambda_l(X)} a_\sigma(X) \quad \text{for} \quad \sigma = 3,4. \qquad (2.20)$$

Notice that we have used different phases $\Lambda_u(X)$ and $\Lambda_l(X)$ for the upper- and lower-layer components, respectively. This is a U(1)×U(1) transformation. These phases can also vary with the orbital index X. [Note: X is not the space coordinate. But, following accepted approximations (see Ref. 6) eventually the sum over the orbital index X will be converted into an integral over space coordinate, invoking the fact that for large magnetic fields, each LLL orbital wave function is highly localized. Hence the above X-dependent transformation corresponds to spatially local gauge transformations.]

Under these local U(1)×U(1) transformations, the one-body Zeeman energy in Eq. (2.9) and the direct part of the Coulomb energy (2.15) are trivially invariant since they involve only the squared modulus of $a_\sigma(X)$. So is the first part (proportional to E^s) of the exchange Coulomb energy (2.16). But the tunneling energy in Eq. (2.9) and the second piece of the exchange energy (2.16), which involves exchange Coulomb interaction E^d between different layers, are invariant only if

$$\Lambda_u(X) = \Lambda_l(X) = \Lambda(X). \qquad (2.21)$$

Thus the full energy of the double-layer system enjoys only a U(1) subgroup of U(1)×U(1) defined in (2.20)—a subgroup where all four components of a_σ are transformed by the *same* phase. This is the U(1) gauge invariance modulo by which our CP³ spinors are defined.

Consider, however, what would happen if we had very widely separated $\nu = 1$ layers (the separation $d \to \infty$). Then each can have its own two-component spin texture described

by a CP¹ system [equivalent to a nonlinear O(3) σ model] with its own U(1) gauge symmetry (see Refs. 5 and 11). The well-separated pair of layers should obey U(1)×U(1) gauge symmetry. Our derivation shows a similar effect. When $d \to \infty$, both the tunneling parameter t in (2.9) and the interlayer Coulomb potential v^d involved in Eq. (2.16) would vanish and the full U(1)×U(1) gauge invariance would indeed be restored. We will see later that this reduced gauge symmetry of a double-layer system at finite separation has consequences in terms of what types of finite energy excitations are permitted in it as compared to a pair of isolated single layers.

III. GRADIENT EXPANSION AND THE CP³ FIELD THEORY

To rewrite the energy expression (2.19) in a continuum field theory language, we proceed following Moon *et al.*[6] and convert sums over the LLL label X into an integral over space. Clearly the one-body energy (2.9), which involves only a single sum over the index X, will become a local term, i.e., a spatial integral over the one-body energy density. But the Coulomb term (2.14) containing a double sum over X_1 and X_2 will become a nonlocal term involving a double integral over some coordinates x_1 and x_2. For long-wavelength excitations one then makes the usual gradient expansion. Expand the spinor for X_2 as

$$a_\sigma(X_2) = a_\sigma(X_1) + (X_2 - X_1)\frac{\partial}{\partial X_1}a_\sigma(X_1) + \cdots. \qquad (3.1)$$

Up till now we found the energy of textures that were y independent.

Now we will invoke the isotropy of the basic system in the x-y plane and generalize this expression for arbitrary textures. This is done by making the replacement

$$\sum_X \to \frac{1}{2\pi l^2}\int d^2r \qquad (3.2)$$

and by replacing x derivatives by gradients. Insert the above expansion (3.1) into the Coulomb energy expressions (2.13)–(2.16). Keep terms only up to order $\partial^2_{X_1}$ and replace the sum Σ_{X_1} by an integral over space as indicated. (These steps are given in the work by Moon *et al.*[6] for the simpler spinless double-layer case). The result for our problem is the following local expression for the total energy (2.19), with overall constants subtracted:

$$E[a_\sigma] = \frac{1}{2\pi l^2}\int d^2r[\tilde{g}(|a_1|^2 - |a_2|^2 + |a_3|^2 - |a_4|^2) - t(a_1 a_3^* + a_2 a_4^* + \text{H.c.})]$$

$$+ \beta_m \int d^2r[F_u(\vec{r}) - F_l(\vec{r})]^2 + 2\rho^s \int d^2r\left[\sum_{i=1,4}[\partial_\mu a^{i*}(\vec{r})\partial^\mu a^i(\vec{r})] + \sum_{i=1,4} a^{i*}(\vec{r})\partial_\mu a^i(\vec{r})^2\right]$$

$$+ (\rho^d - \rho^s)\int d^2r[a^1 a^{3*}\vec{\nabla}^2(a^3 a^{1*}) + a^1 a^{4*}\vec{\nabla}^2(a^4 a^{1*}) + a^2 a^{3*}\vec{\nabla}^2(a^3 a^{2*}) + a^2 a^{4*}\vec{\nabla}^2(a^4 a^{2*}) + \text{H.c.}],$$

$$(3.3)$$

where the constants appearing above are defined by

$$\beta_m = \frac{1}{4} \sum_{(X_2-X_1)} \{[E^d(X_2-X_1)-E^s(X_2-X_1)]$$

$$-[D^d(X_2-X_1)-D^s(X_2-X_1)]\}, \qquad (3.4)$$

$$\rho^s = \frac{1}{2} \sum_{(X_2-X_1)} \frac{(X_2-X_1)^2}{2} E^s(X_2-X_1), \qquad (3.5)$$

$$\rho^d = \frac{1}{2} \sum_{(X_2-X_1)} \frac{(X_2-X_1)^2}{2} E^d(X_2-X_1). \qquad (3.6)$$

These constants are again the same as given by Moon *et al.*[6] in the spinless double-layer problem. The term involving β represents the ''capacitance energy'' of the double-layer system. It is proportional to the square of $F_u(\vec{r})-F_l(\vec{r})$, which gives the difference in charge density between the two layers. The constants ρ^s and ρ^d represent spin-pseudospin stiffness coming from intralayer and interlayer Coulomb interactions, respectively.

This energy functional (3.3) will act as the effective classical Hamiltonian to be minimized to find different textured solutions. The ground state will correspond to a spatially uniform texture, and so can be obtained by minimizing the gradient-free terms in Eq. (3.3). This is acheived by the spinor $a_\sigma(X)=(1/\sqrt{2})(0,1,0,1)$. The one-body Zeeman and tunneling energies are clearly minimized by this choice since the spin is polarized ''down'' in both layers and the psuedospin is along the x direction, i.e., a layer-symmetric state. This choice also minimizes the capacitance energy since it has equal occupancy in the two layers $F_u=F_l=\frac{1}{2}$.

Moving on to excited states with nontrivial textures, these are obtained by extremizing the full energy functional (3.3). Note that Eq. (3.3) including its gradient terms is still gauge invariant under the local U(1) transformation mentioned earlier,

$$a_\sigma(X) \rightarrow e^{i\Lambda(X)} a_\sigma(X) \qquad (3.7)$$

so that this is still a CP^3 theory. In fact the term proportional to the isotropic spin-pseudospin stiffness ρ^s, namely,

$$E_{CP} \equiv 2\rho^s \int d^2r \left[\sum_{i=1,4} [\partial_\mu a^{i*}(\vec{r}) \partial^\mu a^i(\vec{r})] \right.$$

$$\left. + \sum_{i=1,4} a^{i*}(\vec{r}) \partial_\mu a^i(\vec{r})^2 \right] \qquad (3.8)$$

is the Euclidean action for the prototype minimal CP^3 theory.[10] Indeed, in the limit where the layer separation d is zero, this E_{CP} will be the only surviving term from the Coulomb energy in Eq. (3.3) since the interlayer and interlayer Coulomb potentials will become equal ($v^s=v^d$) and hence both β and $\rho^s-\rho^d$ will vanish.

The properties of this prototype CP^3 system and its topological solitons are well known.[10,11] Let us briefly recall those salient features that will be of relevance to us. Define a gauge field A_μ as follows:

$$A_\mu \equiv i \sum_\sigma [a_\sigma^* \partial_\mu a_\sigma]. \qquad (3.9)$$

Clearly under the gauge transformation (3.7),

$$A_\mu \rightarrow A_\mu - \partial_\mu \Lambda. \qquad (3.10)$$

The energy E_{CP} can then be written in a manifestly gauge invariant manner as

$$E_{CP} \equiv 2\rho^s \int d^2r \sum_{\sigma=1}^4 \sum_{\mu=1}^2 |D_\mu a^\sigma(\vec{r})|^2, \qquad (3.11)$$

where $D_\mu = \partial_\mu + iA_\mu$ is the covariant derivative of the U(1) gauge transformation. Then any finite energy field must obey, as $\vec{r} \rightarrow \infty$, the boundary condition

$$D_\mu a_\sigma = (\partial_\mu + iA_\mu) a_\sigma = 0. \qquad (3.12)$$

Since A_μ is independent of the spinor index σ, this implies (see Ref. 11) that as $\vec{r} \rightarrow \infty$,

$$a_\sigma \rightarrow b_\sigma e^{i\phi(\theta)}, \qquad (3.13)$$

where b_σ is some constant spinor. The important point is that all four components of a_σ have the same asymptotic phase ϕ, which may depend on the spatial angle θ. The underlying reason is that the system is invariant under the same single U(1) gauge transformation (3.7) acting on all the four components of a_σ. Finally, the phase function $e^{i\phi(\theta)}$ as $\vec{r} \rightarrow \infty$ is a mapping of one circle (spatial infinity) into another [the U(1) group manifold], and can therefore be divided into homotopy classes characterized by a winding number

$$Q = -\frac{i}{2\pi} \int d^2r [\epsilon_{\mu\nu}(D_\mu a_\sigma)^*(D_\mu a_\sigma)]. \qquad (3.14)$$

For more details supporting these results see Ref. 11. Exact soliton solutions for the minimal CP^3 system also known analytically in terms of analytic functions. Those will not, however, hold for our full system (3.3), which has to be used when the layer separation $d \neq 0$. The solutions will have to be obtained numerically by using appropriate ansatz. But the boundary condition (3.13) and the winding-number classification will still hold. They can be used to decide what forms of intertwined spin-pseudospin solitons are permitted in double layers.

An important consequence of the common phase boundary condition (3.13) is that certain spin textures one can imagine having for two separate single layers are not permissible in the double-layer system. Consider a single layer at $\nu=1$ carrying a skyrmion with winding number n. This is a finite energy configuration which can be described by a two-component spinor, say,

$$\begin{pmatrix} \lambda(r) \\ f(r)e^{in\theta} \end{pmatrix},$$

obeying boundary conditions as $r \rightarrow \infty$ given by

$$\lambda(r) \rightarrow 0,$$

$$f(r) \to 1,$$

and as $r \to 0$

$$\lambda(r) \to 1,$$

$$f(r) \to 0. \tag{3.15}$$

One can have two such layers, widely separated, with two different spin-winding numbers n and m, respectively. Nothing prohibits this. However, suppose the two layers are part of a $\nu = 1$ double-layer system at finite d, and are described by a CP^3 four-spinor

$$\frac{1}{\sqrt{2}} \begin{pmatrix} \lambda_1(r) \\ f_1(r) e^{im\theta} \\ \lambda_2(r) \\ f_2(r) e^{in\theta} \end{pmatrix}. \tag{3.16}$$

This would violate the condition (3.13) since asymptotically the second and fourth components would have different phase functions. Such a texture is forbidden as per our analysis and indeed if one calculates its energy by inserting it in Eq. (3.3) one will find the energy diverging logarithmically. The divergence comes from the angular derivative of $(1/r^2)\partial_\theta^2$ contained in the Laplacians ∇^2 in Eq. (3.3). That yields a contribution to the energy density proportional to

$$\frac{n^2 + m^2}{2r^2} - \frac{(n+m)^2}{4r^2} \tag{3.17}$$

as $r \to \infty$, which will lead to a logarithmic divergence unless $n = m$. At the theoretical level the reason for this can be traced to the reduction of gauge symmetry discussed earlier, from $U(1) \times U(1)$ to $U(1)$ when two layers are together.

Keeping in mind this constraint of equal spin-winding numbers in each layer, let us illustrate nontrivially intertwined spin-pseudospin configurations with the following example that is allowed:

$$A \begin{pmatrix} \lambda_1 \\ z-b \\ \lambda_2 \\ z+b \end{pmatrix}. \tag{3.18}$$

Here $\lambda_{1,2}$ and b are nonzero constants while z is the complex coordinate on the plane. $A = (\lambda_1^2 + |z-b|^2 + \lambda_2^2 + |z+b|^2)^{-1/2}$ is the normalization factor. Asymptotically, the first and third components of Eq. (3.18) both behave as $(1/\sqrt{2})e^{i\theta}$ while the other two components vanish. This is therefore a permitted (energetically finite) CP^3 configuration with winding number $Q = 1$.

One can see that this example is so designed that within each layer the spin texture looks like that of a single skyrmion, while at the same time it is also a ''bimeron'' in the ''psuedospin of the down-spin component'' [contained in the second and fourth components of the four-spinor of ex-

ample (3.18). See Ref. 13 for more on bimerons]. But, we should remember that the the upper and lower layers are not separately normalized in the example (3.18). As $\vec{r}$ varies so does the relative charge density in the two layers. Thus the spin vector in the upper (or lower) layer in example (3.18) will not be a unit vector at every point unless it is is locally renormalized by the charge density of that layer at that point. Similarly, while the pseudospin of the down-spin component in the example (3.18) forms a bimeron, this pseudospin will also be a unit vector at each $\vec{r}$ only after being renormalized by the down-spin density, which varies from point to point. Such renormalization can be achieved by writing any general CP^3 four-spinor (2.1) in terms of spin and pseudospin polar angles:

$$a_\sigma = \begin{pmatrix} \cos\dfrac{\alpha}{2} \cos\dfrac{\theta_u}{2} \\[2ex] \cos\dfrac{\alpha}{2} \sin\dfrac{\theta_u}{2} e^{i\phi_u} \\[2ex] \sin\dfrac{\alpha}{2} \cos\dfrac{\theta_l}{2} e^{i\beta} \\[2ex] \sin\dfrac{\alpha}{2} \sin\dfrac{\theta_l}{2} e^{i(\beta+\phi_l)} \end{pmatrix}, \tag{3.19}$$

where the angles $\theta_{u,l}$, and $\phi_{u,l}$ are the polar angles of the spin in the upper (lower) layer while α and β are the polar angles of the pseudospin, each of which is a the function of the coordinate $\vec{r}$. (Recall that the CP^3 spinor has six real gauge invariant degrees of freedom.) Suppose we tentatively define, using these polar angles, the familiar expression for the spin-skyrmion number in each layer by

$$n_{u,l} = \frac{1}{4\pi} \int d^2r \, \epsilon_{\mu\nu} \partial_\mu (\cos\theta_{u,l}) \partial_\nu(\phi_{u,l}). \tag{3.20}$$

One can then verify that the configuration (3.18) indeed yields unit spin-winding numbers $n_{u,l} = 1$ in each layer.

Similarly, to get the pseudospin winding number one uses an alternate parametrization of the same four-spinor:

$$a_\sigma = \begin{pmatrix} \cos\dfrac{\alpha_\uparrow}{2} \cos\dfrac{\theta_s}{2} \\[2ex] \cos\dfrac{\alpha_\downarrow}{2} \sin\dfrac{\theta_s}{2} e^{i\phi_s} \\[2ex] \sin\dfrac{\alpha_\uparrow}{2} \cos\dfrac{\theta_s}{2} e^{i\beta_\uparrow} \\[2ex] \sin\dfrac{\alpha_\downarrow}{2} \sin\dfrac{\theta_s}{2} e^{i(\beta_\downarrow+\phi_s)} \end{pmatrix}. \tag{3.21}$$

Then the pseudospin winding number for the down-spin component, for example, can be written as

$$n_{ps}(\downarrow) = \frac{1}{4\pi} \int d^2r \, \epsilon_{\mu\nu} \partial_\mu (\cos\alpha_\downarrow) \partial_\nu(\beta_\downarrow). \tag{3.22}$$

Again, the example (3.18) happens to yield $n_{ps}(\downarrow)=1$ in addition to, as we have seen, $n_{u,l}=1$. Thus the example (3.18) illustrates an intertwined spin-pseudospin topological configuration, containing the spin texture of a skyrmion in each layer and the pseudospin texture of a bimeron in the down-spin component.

One should however be cautioned that there is only one true topological charge Q in the full CP^3 theory, given in Eq. (3.14). Although the above example (3.18) contains the texture of two skyrmions and a bimeron, its CP^3 topological index Q obtained by inserting it into Eq. (3.14) will come out to be not 3, but unity. The separate subcharges for spin and pseudospin defined in Eqs. (3.20) and (3.22) in general do not have the same characteristics as they would have had for skyrmions in a single layer or bimeron in a spinless problem. Although in the above example these separate spin and pseudospin winding numbers turn out to be integers, in general they need not be integers, or more importantly, be conserved in time. They are not protected by homotopy considerations in our full four-component theory. The angles $\theta_{u,l}$, etc., used in Eq. (3.19) cannot always be obtained from the original components a_σ of the four-spinor (2.1), since they are not defined at those singular points where $\alpha=\pi,0$, respectively. A similar remark holds for the other angles used above. The numbers $n_{u,l}$ and n_{ps} can change in time due to leakages through such singular points. It is, however, interesting to note that the exact CP^3 winding number can be rewritten in expanded form using the angles defined in Eq. (3.19) into parts that can be attributed to winding of spin and pseudospins. This also brings out the intertwining of spin-psedospin texture. We have

$$Q=\frac{1}{4\pi}\int d\mathbf{r}\,\epsilon^{\mu\nu}\{\partial_\mu(\cos\alpha)[\tfrac{1}{2}(1-\cos\theta_u)\partial_\nu\phi_u$$

$$-\tfrac{1}{2}(1-\cos\theta_l)\partial_\nu\phi_l-\partial_\nu\beta]-F_u(\vec{r})\partial_\mu(\cos\theta_u)\partial_\nu\phi_u$$

$$-F_l(\vec{r})\partial_\mu(\cos\theta_l)\partial_\nu\phi_l\},\tag{3.23}$$

where $F_u(\vec{r})=(1/2)[1+\cos\alpha(\vec{r})]$ and $F_l(\vec{r})=(1/2)[1-\cos\alpha(\vec{r})]$ are, respectively, the same quantities as in Eqs. (2.10) and (2.11) and denote the number density in the top and bottom layers. For the spinless (spins fully frozen) case one can set θ_u, θ_l, ϕ_u, and ϕ_l to be constants. Then one will recover the pseudospin topological charge formula

$$n_{ps}=-\frac{1}{4\pi}\int d\mathbf{r}\,\epsilon^{\mu\nu}\partial_\mu(\cos\alpha)\partial_\nu\beta.\tag{3.24}$$

Similarly for a single-layer (say the upper-layer) case one can set $\alpha=0$ and recover the spin winding-number formula

$$n_u=-\frac{1}{4\pi}\int d\mathbf{r}\,\epsilon^{\mu\nu}\partial_\mu(\cos\theta_u)\partial_\nu\phi_u.\tag{3.25}$$

In general, where both spin and pseudospin have some intertwining texture, the full topological charge will receive contributions from the windings of all these, as given in Eq. (3.23).

Finally, the very simple example (3.18) not only illustrates a nontrivial intertwining texture, it is also an exact solution of the prototype CP^3 theory (3.8) since its components are analytic functions (see Ref. 11). But, for our full theory in the presence of a nonzero layer separation and with Zeeman and tunneling energies, classical solutions minimize the full energy functional (3.3), have to be obtained numerically by solving the nonlinear coupled partial differential equations that the minimization conditions yield. The simple analytical example (3.18), however, will guide us in setting up the desired ansatz for the numerical solution with appropriate boundary conditions so that intertwined textures which are nontrivially wound in both spin and pseudospin can be obtained for our full theory. An illustrative family of such solutions is obtained in the next section.

IV. FIELD EQUATIONS AND THEIR SOLUTIONS

Classical solutions that minimize the full energy functional (3.3) have to be obtained numerically. To do this we use the parametrization of the spinor components of the form

$$a_\sigma=\begin{pmatrix}\cos\dfrac{\alpha}{2}\cos\dfrac{\theta_u}{2}\\[2mm]\cos\dfrac{\alpha}{2}\sin\dfrac{\theta_u}{2}e^{i\phi_u}\\[2mm]0\\[2mm]\sin\dfrac{\alpha}{2}e^{i\phi_l}\end{pmatrix}.\tag{4.1}$$

One can see that this is a sub-family of the general case in Eq. (3.19), where for simplicity we have set θ_l equal to π and $\beta=0$.

We will look for numerical solutions that would have corresponded if the energy had been of the simple prototype functional (3.18), to its exact analytic solution

$$A\begin{pmatrix}\lambda\\z-b\\0\\z+b\end{pmatrix}.\tag{4.2}$$

This configuration represents a spin skyrmion in the upper layer intertwined with a bimeron in the "pseudospin of the downspin component." It does not have any nontrivial winding in the real spin of the lower layer (though the fourth component in the spinor varies over the coordinate space the spin will always be down). To ensure that our numerical solutions have the same topological properties as well as similar profiles as the prototype spinor (4.2) we impose the same boundary conditions on the components of the former as obtained in the latter, both asymptotically and at the meron centers $x=\pm b$.

In terms of the ansatz (4.1) the local energy functional (3.3) takes on the form

$$E_C = \beta_m \int d\vec{r}\cos^2\alpha + 2\rho^s \int d\vec{r}\left[\frac{1}{4}\left((\vec{\nabla}\alpha)^2 + \cos^2\frac{\alpha}{2}(\vec{\nabla}\theta_u)^2\right) + \frac{1}{4}[(1+\cos\alpha)(1-\cos\theta_u)(\vec{\nabla}\phi_u)^2 + 2(1-\cos\alpha)(\vec{\nabla}\phi_l)^2]\right.$$

$$-\frac{1}{16}[(1+\cos\alpha)^2(1-\cos\theta_u)^2(\vec{\nabla}\phi_u)^2 + 4(1-\cos\alpha)^2(\vec{\nabla}\phi_l)^2 + 4(1-\cos^2\alpha)(1-\cos\theta_u)\vec{\nabla}\phi_u\cdot\vec{\nabla}\phi_l]\Big]$$

$$+(\rho^s-\rho^l)\int d\vec{r}\left[\frac{1}{2}[(\vec{\nabla}\cos\alpha)^2 - (\vec{\nabla}\alpha)^2] + \sin^2\alpha\left(-\frac{1}{8}(\vec{\nabla}\theta_1)^2 - \frac{1}{4}[(1-\cos\theta_u)(\vec{\nabla}\phi_u)^2\right.\right.$$

$$+2(\vec{\nabla}\phi_l)^2 + 2(1-\cos\theta_u)\vec{\nabla}\phi_u\cdot\vec{\nabla}\phi_l]\Big)\Big]. \tag{4.3}$$

This energy functional has to be minimized with respect to all the angle fields in the anstatz. As we did in our earlier work on the spinless problem,[13] here too we will use the bipolar coordinate system[16] to describe the spatial plane:

$$\eta = \ln|z-a| - \ln|z+a|; \quad \phi = \arg(z-a) - \arg(z+a). \tag{4.4}$$

We have already elaborated in Ref. 13 the advantages of this coordinate system when one has to impose the bimeron-type boundary conditions. However, here the advantages of introducing such an unfamiliar coordinate system is not as much as in the simple spinless bilayer problem of Ref. 13 because the ansatz here is not symmetric between the two layers. Consequently unlike the spinless case $\cos\alpha$ is no more antisymmetric about $\eta=0$ axis. All these features along with the fact that the energy minimization unavoidably requires solving coupled nonlinear partial diffential equations (PDE) render the numerical exercise much more complicated here. What we have done under these circumstances is the following.

We have solved the field equations numerically for the case where just the capacitance term is added to the minimal CP^3 energy. From our earlier calculations we know that this term is going to change the solutions considerably. The terms in each equation with the coefficient $(\rho^s-\rho^l)$, which accounts for the anisotropy in the exchange energy is not included in the process of numerical integration. As a justification of such simplification we can say that the anisotropic terms that involve higher-order gradients of the spin pseudospin field will have a less pronounced effect compared to the capacitance term on the solutions. This has been graphically shown in Figs. 1 and 2 of our earlier work.[13] Even after this drastic simplification we are still left with solving four coupled nonlinear PDE's. For example, the equation which is obtained by extremizing the energy with respect to $\cos\alpha$ is

$$\left(\frac{\delta E_C}{\delta\cos\alpha}\right)_{\rho^s=\rho^l} = 2\beta_m Q_s^2\cos\alpha + \rho^s\left[-2\frac{\cos\alpha(\vec{\nabla}\cos\alpha)^2}{(1-\cos^2\alpha)^2}\right.$$

$$-2\frac{\nabla^2\cos\alpha}{1-\cos^2\alpha} + (1-\cos\theta_u)(\vec{\nabla}\phi_u)^2$$

$$-2(\vec{\nabla}\phi_l)^2 - \frac{1}{4}(1+\cos\alpha)(1-\cos\theta_u)^2$$

$$\times(\vec{\nabla}\phi_u)^2 + (1-\cos\alpha)(\vec{\nabla}\phi_l)^2$$

$$+\cos\alpha(1-\cos\theta_u)(\vec{\nabla}\phi_u\cdot\vec{\nabla}\phi_l)\Big] = 0, \tag{4.5}$$

where

$$Q_s^2(\eta,\phi) = \frac{b^2}{(\cosh\eta - \cos\phi)^2} \tag{4.6}$$

is the Jacobian of this coordinate transformation and all gradient operators are defined in the bipolar-coordinate system.[16] Similarly we will have three more equations obtained by extremizing the energy functional with respect to θ_u, ϕ_u, and ϕ_l and then writing the resulting equations in bipolar coordinates. We will not display them here.
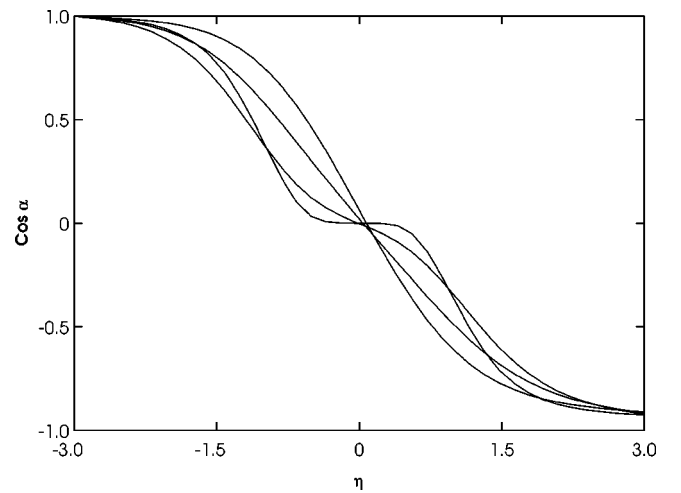

FIG. 1. The solution $\cos\alpha(\eta)$ of the field equations for a set of values for ϕ. The curves correspond, as one goes inwards, to $\phi = 0.09\pi, 0.36\pi, 0.63\pi, 0.90\pi$, respectively, where the outermost one corresponds to ϕ equal to 0.09π. The layer separation d is equal to $0.6l$ and bimeron separation b is equal to $2.5l$. The value of λ in the analytic ansatz is $1l$.

A. Numerical procedure

The numerical procedure is almost the same as that in Ref. 13. Here also one can see that the Jacobian factor Q_s in the first term of Eq. (4.5) is singular at the point ($\eta = 0, \phi = 0$). The behavior of $\cos \alpha$ near this point is also going to be same as the behavior of m_z in Ref. 13. The major difference compared to the earlier problem, however, comes from the fact that it is no longer sufficient to find out the solutions in one quadrant and get the rest from symmetry considerations. We have to solve this problem on both sides of the $\eta = 0$ axis since our starting ansatz solution is not completely antisymmetric around $\eta = 0$. During the numerical work one also has to be careful about the different branches of the angles $\phi_{u,l}$. As one needs to integrate the equations on the both sides of the $\eta = 0$ axis the size of the mesh on which we have to discretize the field equations becomes larger compared to the earlier case of spin-frozen double-layer problem.[13] Also here we have to solve four coupled PDE's simultaneously. This simultaneous increase in the number of lattice points as well as independent fields demands that we have to invert a huge determinant in the Newton-Raphson procedure[17] while improving over the initial guess solution. This forces us to increase the lattice constants of the mesh slightly compared to what we have done in our earlier work.[13] However, we have checked that the error introduced in this way is not very high. In the next subsection we shall present our results along with the discussion.

B. Results and discussion

Our solutions of Eq. (4.5) along with the other three field equations yield the spatial behavior of the CP^3 fields parametrized in term of the angles α, β, $\theta_{u,l}$, and $\phi_{u,l}$. The calculations are done iteratively. We start with the simple analytical spinor (4.2), which is the exact solution when the capacitance and anisotropy terms in the energy (4.6) are absent. Then the capacitance term in the equation is introduced in small steps and the corresponding solution obtained numerically. We have performed several calculations each starting from different initial values of the constants λ and b. The constant λ represents the starting value of the first component of the spinor in the iteration process. It stands for the spin-skyrmion size in the CP^3 limit, but when subsequent iterations are performed in the presence of other energy terms, it is replaced by a space-dependent solution. But the parameter b is fixed for a given calculational run. It represents the meron separation and enters into Eq. (4.5) explicitly through the first (capacitance) term. While we do calculations for different values of b, the optimal value of b will have to be obtained by minimizing the energy with respect to it. We will return to this point later.

We present below the salient features of our numerical results. The major feature we want our numerical solution to have is the intertwining of the spin skyrmion with the pseudospin bimeron. We would also like to show the leakage of electrons of either spin from one layer to another as we move in space, as a fallout of this intertwining. To show this, we have plotted both $\cos \alpha$ and $\cos \alpha_\downarrow$ as a function of η for a set of values of the angle ϕ in Fig. 1 and Fig. 2, respectively.
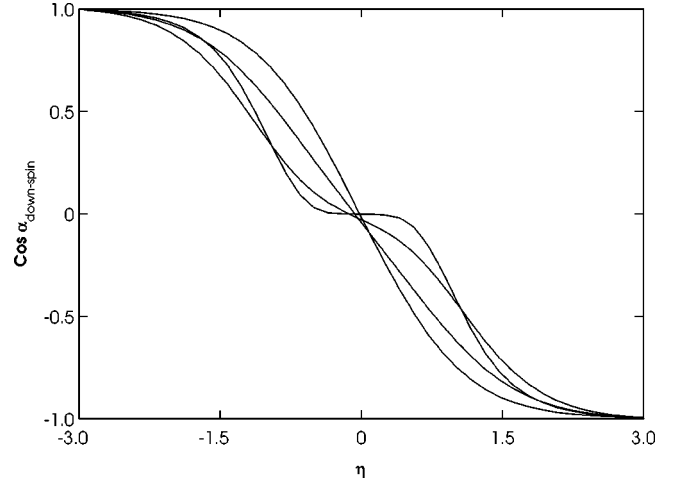

FIG. 2. The plot of $\cos \alpha_\downarrow(\eta)$ (down-spin) for a set of values for ϕ. The curves correspond, as one goes inward, to $\phi = 0.09\pi, 0.36\pi, 0.63\pi, 0.90\pi$, respectively, where the outermost curve corresponds to ϕ equal to 0.09π. The layer separation d is again equal to $0.6l$ and bimeron separation b is equal to $2.5l$. The value of λ in the analytic ansatz is also $1l$.

These solutions correspond to layer separation $d = 0.6l$, bimeron center separation $b = 2.5l$, and start from an initial value of $\lambda = 1$ in the starting trial solution (4.2). The sequence of curves shown correspond to ϕ equal to 0.09π, 0.36π, 0.63π, and 0.90π, respectively, with the outermost one belonging to ϕ equal to 0.09π. As we have discussed earlier,[13] note from the definition of the bipolar coordinates that spatial infinity in x-y plane corresponds to η and ϕ both equal to zero. As we approach this point in the (ϕ, η) plane, the solution should damp exponentially as $\exp(-\kappa/\sqrt{\eta^2 + \phi^2})$, where

$$\kappa = \sqrt{\frac{2\beta}{\rho_A}} b. \tag{4.7}$$

Correspondingly we see in Figs. 1 and 2 that the low-ϕ curves rise very slowly as η increases away from zero.

The interesting point to note about these solutions is that in Fig. 1 $\cos \alpha$ approaches different (absolute) asymptotic values as η approaches $\pm \infty$. (These are the centers of the two merons that form the bimeron. Although computational limitations allow us to go only up to values of $\eta = \pm 3$, it is clear from the figure that asymptotic behavior has been obtained.) This asymptotic behavior is extracted directly from the analytic ansatz (4.2) and implies the leakage from the pseudospin to spin. It is useful to remember at this point that we have a bimeron only in the ''pseudospin of the down-spin component,'' whereas $\cos \alpha$ represents the z component of the total pseudospin. This is realized in Fig. 2. Here $\cos \alpha_\downarrow$ (down-spin) represents the z component of the ''pseudospin of the down-spin component.'' It is completely antisymmetric about $\eta = 0$ and approaches ± 1 as η approaches $\pm \infty$. This behavior is same as the behavior of m_z in the spinless bilayer case. This is how we can extract from our results the pure bimeron by suitably partitioning the pseudospin into different spin components.
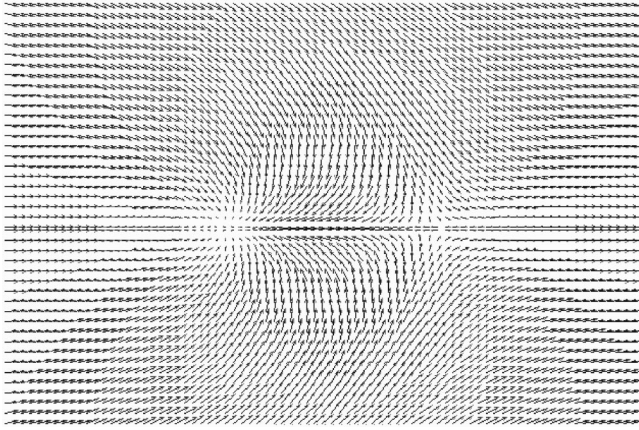
FIG. 3. This figure gives the magnitude and direction of x-y projection of the total pseudospin at different points on the plane. The magnitude of each arrow at a given point is $\sin \alpha$ and its angle with the x axis is $\phi_l - \phi_u$ at that point. The layer separation and the bimeron separation are same as in Figs. 1 and 2.

Since bipolar coordinates are not very familiar we have given an alternate representation of the above results through a vector plot in the physical x-y space in Figs. 3 and 4. The values of the parameters in these figures are same as those in Fig. 1. In Fig. 3 the magnitude of each arrow gives the absolute value of the transvere component of the total pseudospin $\sin \alpha$ and its angle with the x axis gives $\phi_u - \phi_l$. One should note in this regard $\phi_u - \phi_l = \beta_\downarrow$ in the other parametrization. Here also one can see the length of the arrow does not quite vanish in one of the bimeron centers and makes this construction singular at this point. However, when we look at Fig. 4 where the magnitude of each arrow is $\sin \alpha_\downarrow$ and the angle is again $\phi_u - \phi_l$, the magnitude of the arrow vanishes at each bimeron center and the profile is no longer singular. This makes Fig. 4 identical to the vector plot of the bimeron pseudospin in the pure layer case.[15,13]
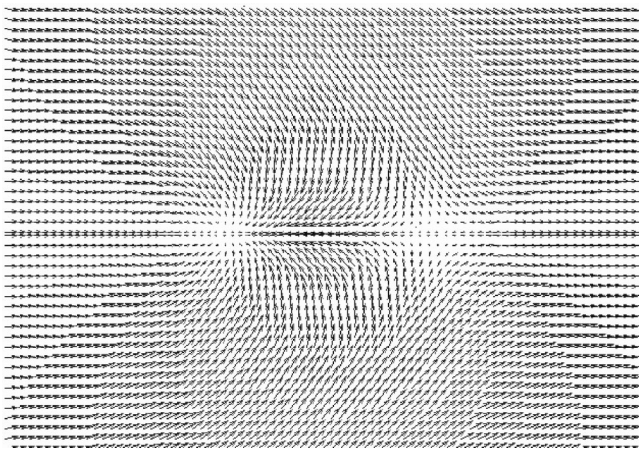

FIG. 4. This figure gives the magnitude and direction of x-y projection of the ''pseudospin in the down-spin component'' at different points on the plane. The magnitude of each arrow at a given point is $\sin \alpha_\downarrow$ and its angle with the the x axis is $\beta_\downarrow$ at that point. The layer separation and the bimeron separation are same as in Figs. 1 and 2.
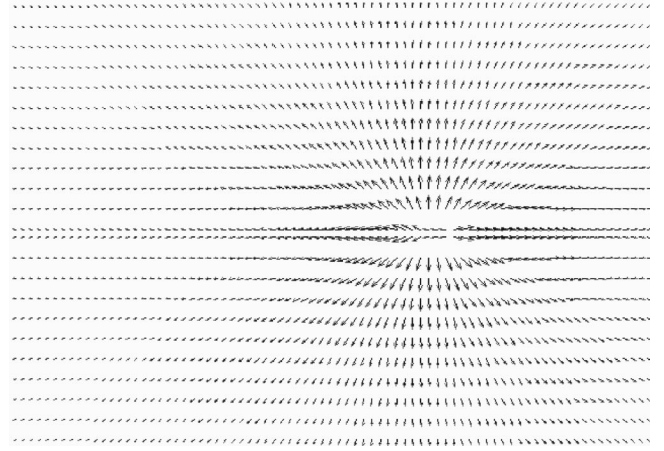

FIG. 5. This figure gives the magnitude and direction of x-y projection of the spin in the upper layer at different points on the plane. At each point the magnitude of the arrow gives $\sin \theta_u$ and its direction with the x axis gives ϕ_u at that point. The layer separation and the bimeron separation and initial λ are the same as in the earlier figures.

In Fig. 5 we have given a similar vector plot for the spin skyrmion in the upper layer. Here the length of the each arrow corresponds to the planar projection of the spin in the upper layer ($\sin \theta_u$) and the its direction gives the azimuthal angle (ϕ_u) of the projected vector. This picture very clearly points out how the skyrmion winds in the azimuthal plane about its center at $x = b$. Here also the layer separation d and the starting values of b and λ are the same as those in Fig. 1. This set of parameters represents a typical example.

Last, we have evaluated the energy of these solutions for a set of values of the meron separation parameter b. The optimal value of b should be obtained by minimizing the full energy as a function of b. But if we include only the capacitance term and the (pseudo)spin-stiffness gradient terms in our energy, these will not lead to a nonzero b, i.e., the textures will want to shrink to zero size. The reason is that under rescaling, the capacitance term grows proportional to the square of the scale while the gradient terms are scale invariant. Of course a change in b will not result in just an overall rescaling of the solution. The shape of the solution will also change since b occurs as a constant multiplying the capacitance term in the differential equation (4.5). As a result, the b dependence of the gradient and capacitance terms will not be simple, although qualitatively it should still drive the meron separation to zero size. This can be seen in Table I, where we show these energies for ten different values of b for a fixed value of other parameters. As expected the sum of both these energy contributions decreases strongly with decreasing b, thus driving the texture to zero size. In reality however, these two terms are just the first two terms in the gradient expansion of the full energy functional. Higher-order terms in the gradient expansion, if included, will make our nonlinear differential equation even more difficult to solve, but they can offset this tendency to shrink.

In particular, one prominent higher gradient contribution to the energy is the Coulomb interaction between different portions of the topological charge densities. It is given by (see Ref. 8):

TABLE I. Different contributions to the total energy (E_{total}) of spin-pseudospin intertwined solitons for a set of b at a layer separation of $d=0.8l$. Here E_{grad} refers to the gradient energy (isotropic plus anisotropic), while E_{capa} is the capacitance energy and E_{Coul} is the Coulomb interaction energy between topological charge densities. E_{total} is the sum of these three contributions to the energy. The unit of energy is $e^2/\epsilon l$ and the unit of length is l.

b	E_{capa}	E_{grad}	E_{Coul}	E_{total}
4.5	0.285	0.261	0.141	0.687
4.0	0.250	0.251	0.152	0.653
3.5	0.229	0.228	0.168	0.625
3.0	0.205	0.223	0.183	0.611
2.5	0.153	0.227	0.217	0.597
2.3	0.143	0.227	0.225	0.595
2.0	0.126	0.203	0.262	0.591
1.8	0.121	0.192	0.290	0.603
1.5	0.104	0.196	0.328	0.628
1.2	0.091	0.200	0.390	0.681
1.0	0.081	0.192	0.456	0.729

$$E_{Coul} = \frac{1}{2} \int d\vec{r}\, d\vec{r}'\, V(\vec{r} - \vec{r}')\, \delta\rho(\vec{r})\, \delta\rho(\vec{r}'), \qquad (4.8)$$

where $\delta\rho(\vec{r})$ is the CP^3 topological charge density given by the integrand of the right-hand side (r.h.s.) of Eq. (3.14).

Inclusion of the contribution of this term into our differential equation for the texture will introduce a *nonlocal* nonlinear term, which will make it very difficult for us to solve it numerically. We can, however, make the following estimate. We can insert our texture solution, obtained without the Coulomb term, into the Coulomb energy integral and evaluate it as a function of b. This contribution is also shown in the Table I. As expected, the Coulomb repulsion energy E_{Coul} decreases with increasing b. This term would like to keep the merons farther apart and offset the tendency to shrink because of the other terms. Thus one may hope to get

TABLE II. The size (i.e., the optimal meron separation b) and the total energy (E_{total}) at different layer separations d. The unit of energy is $e^2/\epsilon l$ and the unit of length is l.

d	b	E_{total}
0.8	2.0	0.59
0.7	2.2	0.59
0.6	2.3	0.60
0.5	2.4	0.60
0.4	2.5	0.59

an optimal bimeron separation at which the sum of all these three energy contributions will become minimized as a function of b.

In Table I we have presented our calculation for the layer separation $d=0.8l$ where different contributions to the total energy are shown along with their sum, the ''total energy.'' For this particular layer separation a distinct minimum is obtained around $b=2.0l$.

To see whether this behavior is common to other layer separations we have plotted in Fig. 6 the total energy E_{total} as a fuction of bimeron separation b for a set of layer separations. The three sets of points in this figure correspond to three different layer separations, namely d equal to $0.5l$, $0.7l$, and $0.8l$. All these three curves show distict minima for the total energy as a function of bimeron separation. We have also provided in Table II the size (b) and total energy of the optimal bimeron for five values of layer separation.

Notice from Table II that the optimal meron separation b decreases with the increase of layer separation d. For $d=0.8l$ the optimal separation is around $b=2.0l$ and gradually increases to $b=2.5l$ for $d=0.4l$. For the case of pure layer bimeron Brey *et al.* also found[15] a similar behavior. This behavior could be attributed to the following. By lowering the layer separation (decreasing the d/l ratio) one increases the relative importance of Coulomb repulsion among topological charge densities (coming from the intralayer Coulomb energy) to the capacitance term (coming from the
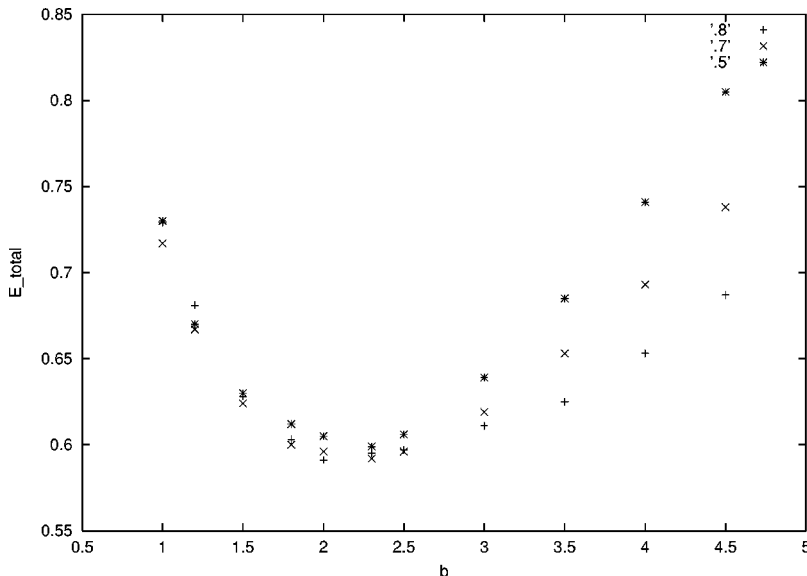

FIG. 6. This figure gives a plot of the total energy E (total) as a function of the bimeron separation b for three different layer separations, namely $d=0.5l$, $0.7l$, and $0.8l$. The unit of energy is again $e^2/\epsilon l$.

interlayer Coulomb repusion). Hence the balancing of the capacitance term by the Coulomb energy will take place at a larger bimeron separation, thereby increasing the size of the bimeron.

We found that resulting energy of these solitons at their optimal sizes varies very little as one changes the layer separation. Although bimerons of larger size at lower layer separations cost higher capacitance energy, the decrease in the Coulomb energy seems to fully offset that. As a result the total energy remains almost the same for different layer separations in the range $d=0.4l$ to $d=0.8l$ that we have studied.

An important question is whether our spin-pseudospin intertwined solution has a lower energy than other candidates among the low-lying excitations. Prominent among these other low-lying excitations with whom such comparisons have to be done are (i) the particle-hole excitations and (ii) purely spin or pseudospin textured solitons. To start with note that in the minimal prototype CP^3 system [valid in the $d=0$ limit; see Eq. (3.8)] the energy is just equal to $E_{CP} = 4\pi\rho^s Q$ (see Ref. 11). Now, a pure-spin skyrmion in, say, one of the layers can also be written in our CP^3 four-spinor notation and will have a CP^3 topological number $Q=1$. So will a bimeron in pseudospin of some spin component. Therefore in the prototype CP^3 system our spin-pseudospin intertwined soliton with $Q=1$ will have the same energy as a purely spin or pseudospin textured soliton with $Q=1$. The intertwining will not cost more energy. All these energies, which are equal, are a quarter of that of a particle-hole pair (see Ref. 8), which costs an energy of $\sqrt{\pi/2} \approx 1.25$ in units of $e^2/\epsilon l$. However, the difference in the energies of these various types of topological excitations come from the additional terms in the full energy E_C due to capacitance, anisotropy, and Coulomb repulsion. As we can see from Table II our intertwined soliton over a range of layer separation has energy around $0.60 e^2/\epsilon l$. It is encouraging that a pair of these excitations would have somewhat lower energy than the particle-hole pair energy of 1.25.

Of course our computational accuracy is not very high, given that we are limited in how many lattice points we can use. One must also improve on the results by solving for the texture functions and their energy after including single particle terms due to the Zeeman coupling and tunneling. Examples of such calculations can be found in the case of $\nu = 2$ by Pardes *et al.*,[14] but not for $\nu=1$ yet to date. Meanwhile, our result for the intertwined soliton at $\nu=1$ and its energy at best raise hopes that they may be competetive as candidates for low-lying excitations in double-layer systems with spin.

*Present address: Institute of Mathematical Sciences, Chennai-600113, India.

*Email address: doug@jnuniv.ernet.in

[1] S.L. Sondhi, A. Karlhede, S.A. Kivelson, and E.H. Rezayi, Phys. Rev. B **47**, 16 419 (1993).

[2] S.E. Barrett, G. Dabbagh, L.N. Pfeiffer, K.W. West, and R. Tycko, Phys. Rev. Lett. **74**, 5112 (1995); J.P. Eisenstein, L.N. Pfeiffer, and K.W. West, Science **268**, 1460 (1995); E.H. Aifer, B.B. Goldberg, and D.A. Broido, Phys. Rev. Lett. **76**, 680 (1996).

[3] J.P. Eisenstein, G.S. Boebinger, L.N. Pfeiffer, K.W. West, and Song He, Phys. Rev. Lett. **68**, 1383 (1992); S.Q. Murphy, J.P. Eisenstein, G.S. Boebinger, L.N. Pfeiffer, and K.W. West, *ibid.* **72**, 728 (1994); Y.W. Suen, L.W. Engel, M.B. Santos, M. Shayegan, and D.C. Tsui, *ibid.* **68**, 1379 (1992); G.S. Boebinger, H.W. Jiang, L.N. Pfeiffer, and K.W. West, *ibid.* **64**, 1793 (1990).

[4] T. Chakraborty and P. Pietilainen, Phys. Rev. Lett. **59**, 2784 (1987); E.H. Rezayi and F.D.M. Haldane, Bull. Am. Phys. Soc. **32**, 892 (1987).

[5] S.M. Girvin and A.H. MacDonald, in *Novel Quantum Liquids in Low-Dimensional Semiconductor Structures*, edited by S.D. Sarma and A. Pinczuk (Wiley, New York, 1995).

[6] K. Moon, H. Mori, Kun Yang, S.M. Girvin, A.H. MacDonald, L. Zheng, D. Yashioka, and Shou-Cheng Zhang, Phys. Rev. B **51**, 5138 (1995).

[7] J.M. Kosterlitz and D.J. Thouless, J. Phys. C **6**, 1181 (1973).

[8] D.P. Arovas, A. Karlhede, and D. Lilliehook, Phys. Rev. B **59**, 13 147 (1999).

[9] Z.F. Ezawa, Phys. Rev. Lett. **82**, 3512 (1999); Phys. Lett. A **249**, 223 (1998).

[10] V. Golo and A.M. Perelemov, Phys. Lett. **99B**, 112 (1978); A. D'Adda, M. Luscher, and P. DiVecchia, Nucl. Phys. B **146**, 63 (1978); H. Eichenherr, *ibid.* **146**, 215 (1978); E. Cremmer and J. Scherk, Phys. Lett. **74B**, 341 (1978); E. Witten, Nucl. Phys. B **149**, 285 (1979).

[11] R. Rajaraman, *Solitons and Instantons* (North Holland, Amsterdam, 1982).

[12] Sankalpa Ghosh and R. Rajaraman, Int. J. Mod. Phys. B **12**, 37 (1998).

[13] Sankalpa Ghosh and R. Rajaraman, Int. J. Mod. Phys. B **12**, 2495 (1998).

[14] B. Paredes, C. Tejedor, L. Brey, and L. Martin-Moreno, Phys. Rev. Lett. **83**, 2250 (1999).

[15] L. Brey, H.A. Fertig, R. Cote, and A.H. MacDonald, Phys. Rev. B **54**, 16 888 (1996).

[16] H. Margenau and G.M. Murphy, *The Mathematics of Physics and Chemistry* (Affiliated East-West Press, New-Delhi, 1971).

[17] William H. Press *et al.*, *Numerical Recipes In Fortran 77*, 2nd ed. (Cambridge University Press, Cambridge, 1992), Chap. 9.